Direct observations of nonmigrating diurnal tides in the equatorial thermosphere

E. R. Talaat[1] and R. S. Lieberman[2]

Received 23 November 2009; revised 7 January 2010; accepted 14 January 2010; published 19 February 2010.

[1] We present direct observations of nonmigrating diurnal tides in the 90–270 km range inferred from the Upper Atmosphere Research Satellite (UARS) wind imaging interferometer (WINDII). A prominent zonal wavenumber 4 appears in daytime zonal winds, extending to 180 km. We interpret this signature as an eastward-propagating diurnal wavenumber 3 (DE3) viewed from the satellite perspective. This evidence of the extended upward propagation of DE3 demonstrates that it acts as a direct coupling agent between the troposphere and the thermosphere (and F-region), in addition to its role in the E-region dynamo. **Citation:** Talaat, E. R., and R. S. Lieberman (2010), Direct observations of nonmigrating diurnal tides in the equatorial thermosphere, *Geophys. Res. Lett.*, *37*, L04803, doi:10.1029/2009GL041845.

1. Introduction

[2] Diurnal tides are forced primarily by radiative and convective heating at tropospheric levels, and by stratospheric ozone heating [*Chapman and Lindzen*, 1970; *Forbes et al.*, 1997; *Lieberman et al.*, 2003]. Due to their exponential increase in amplitude with height, vertically propagating tides are among the most prominent features in the equatorial mesosphere and lower thermosphere (MLT) [*Hays et al.*, 1994; *McLandress et al.*, 1996a]. The associated motions and density variations also induce spatiotemporal modulations of gravity-wave fluxes [*McLandress and Ward*, 1994], atomic oxygen recombination airglow emissions [*Burrage et al.*, 1994], and even modulation of thermospheric nitric oxide [*Oberheide and Forbes*, 2008a].

[3] The most prominent MLT diurnal component is the migrating tide that propagates westward with a zonal wavenumber one, and an angular phase speed equal to the frequency of Earth's rotation, or Ω [*Zhang et al.*, 2006]. The migrating tide is forced by radiative heating in the troposphere and stratosphere [*Chapman and Lindzen*, 1970; *Lieberman et al.*, 2003]. Additional components with phase speeds different from Ω, dubbed nonmigrating tides, are driven by longitudinal variations in radiative and convective heating [*Forbes et al.*, 1997; *Talaat and Lieberman*, 1999; *Hagan and Forbes*, 2002; *Lieberman et al.*, 2007]. The most prominent of these is an eastward-propagating tide with zonal wavenumber 3. This wave, often referred to as DE3, is forced by latent heat release in deep tropospheric convection [*Hagan and Forbes*, 2002]. Satellite observations show that the migrating tide saturates near 95 km and attenuates rapidly above that level [*Lieberman and Hays*, 1994; *McLandress et al.*, 1996b]. However, DE3 continues to grow above 105 km [*Talaat and Lieberman*, 1999; *Oberheide et al.*, 2006].

[4] Longitudinal variations with a zonal wavenumber 4 structure have been reported in satellite observations of numerous F-region parameters such as UV airglow [*Sagawa et al.*, 2005; *Immel et al.*, 2006; *England et al.*, 2006], equatorial electrojet [*Lühr et al.*, 2008], electron density and vertical ion drift [*Kil et al.*, 2008], and the thermospheric zonal wind [*Lühr et al.*, 2007]. Because the observations were made from orbiting satellites over a narrow range of local times, the wavenumber 4 was identified as an eastward-propagating diurnal zonal wavenumber 3 wave, Doppler-shifted to wavenumber 4 in the local-time fixed satellite frame of reference [*Salby*, 1982]. More complete analyses of Challenging Minisatellite Payload (CHAMP) winds have confirmed the presence of DE3 in 400 km zonal winds [*Häusler and Lühr*, 2009].

[5] The plasma anomalies have been shown numerically to arise from modulation of the E-region dynamo by DE3 zonal winds, which in turn alters the equatorial ionospheric "fountain" [*England et al.*, 2006; *Hagan et al.*, 2007]. However, the presence of DE3 in the 400 km zonal wind suggests that the wave itself may propagate vertically from its tropospheric source into the upper thermosphere. *Oberheide and Forbes* [2008b] and *Oberheide et al.* [2009] applied Hough Mode Extensions (HMEs) to DE3 winds and temperatures derived from TIMED measurements. Essentially, this method uses a physics-based model to empirically fit the structure of DE3 winds above 105 km, and DE3 temperatures above 120 km [*Svoboda et al.*, 2005]. *Oberheide et al.* [2009] concluded that observed thermospheric DE3 winds were consistent with empirically fit values, and therefore attributable to direct upward propagation of DE3. *Forbes et al.* [2009] applied the same methodology to CHAMP and Gravity Recovery and Climate Experiment (GRACE) thermospheric temperatures, and concluded that DE3 as well as DE2 propagated directly into the exosphere (350–500 km).

[6] The studies of *Oberheide and Forbes* [2008b] and *Forbes et al.* [2009] relied upon HMEs as proxies for actual tidal measurements in the 120–400 km range. The purpose of this study is to present direct measurements of DE3 winds between the lower and the upper thermosphere. A prominent wave with zonal wavenumber 4 appears in daytime Upper Atmosphere Research Satellite (UARS) wind imaging interferometer (WINDII) winds that we convincingly interpret as DE3. The wave is strongest in the equatorial zonal wind,

[1]Johns Hopkins University Applied Physics Laboratory, Laurel, Maryland, USA.
[2]Colorado Research Associates Division, Northwest Research Associates, Boulder, Colorado, USA.

0094-8276/10/2009GL041845$05.00

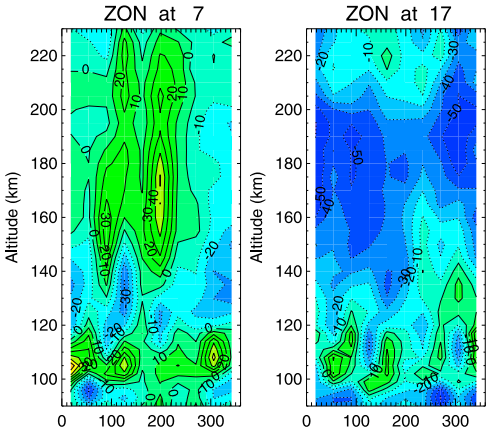

Figure 1. Zonal winds plotted as a function of longitude and altitude at the equator, during Sept-Oct-Nov. Winds are presented at (left) 7 and (right) 17 LST.

but is also coherent in the meridional wind. Zonal wind amplitudes of 10 m s^{-1} persist above 200 km.

2. Data and Analysis

[7] WINDII measured winds and temperatures in the 90–300 km range by sensing the visible region airglow emission from these altitudes. Wind velocities were inferred from small wavelength shifts of the airglow emission (induced by atmospheric motion), viewed from two orthogonal directions. The O(^{1}S) 557.0 nm ("green line") emission spanned 90–200 km, while the 200–300 km region is characterized by the O(^{1}D) 630.0 nm ("red line") emission. A complete discussion of WINDII measurement and errors, and comparisons with correlative data are found in work by *Gault et al.* [1996].

[8] The UARS mission commenced in 1991, and was deactivated in 2005. The bulk of WINDII's measurements were taken between 1992–1995. However, the green line emission was typically observed 4 times per week during the day and only twice a week at night [*McLandress et al.*, 1996b]. The red line measurements were made once per week [*Emmert et al.*, 2001]. As a result, we must composite multiannual data in order to obtain the longitudinal and local time coverage necessary for this study. Winds between 1992–1997 with $K_P \leq 3$ index were collected on altitude surfaces, and gridded for each season in 5° × 36° latitude-longitude bins, and 2-hour local time bins. The standard deviation is computed for each bin, and only data values within 3 standard deviations are retained for the averaged bin value.

[9] Figure 1 shows zonal winds plotted as a function of longitude and altitude at the equator, during September-October-November. Winds are presented at 7 and 17 LST. A prominent wavenumber 4 pattern appears between 100–140 km. Comparison of the two plot shows that between 100–140 km, the patterns are in nearly opposite phase between 90 and 140 km, suggesting a predominantly diurnal variation. Between 140–220 km, the wave 4 component remains visible in the zonal wind maxima at 7 LST that are separated by roughly 100 degrees. Similar longitudinal spacing is observed in the wind minima at 17 LST. The corresponding meridional winds (not shown) exhibit structures that are quite different from the zonal winds. The prevailing waves are zonal wavenumbers 2 and 3, with a hint of zonal wavenumber 4 between 150–200 km.

[10] Gridded zonal and meridional winds were averaged between 10°S–10°N, and Fourier transformed with respect to longitude. Figure 2 shows the vertical structure of the zonal wavenumber 4 component of zonal and meridional winds. The zonal wind component of the wave attains an amplitude of 20 m s^{-1} at 100 km, and is considerably stronger in the lower thermosphere (90–130 km) than the meridional wind. Above 130 km the zonal and meridional amplitudes are comparable, maximizing at 10 m s^{-1}. The phase increases with height monotonically, tilting eastward and indicating a wavelength of about 40 km in the lower thermosphere. The phase of the meridional wind is shifted downward in altitude relative to the zonal wind. At 100 km the meridional wind leads the zonal wind by about 40°, or nearly a half-cycle. At 170 km, the phase offset between the meridional and zonal wind has decreased to about 15°, less than 1/4 cycle.

[11] As mentioned previously, the zonal wavenumber associated with satellite measurements at a fixed local time may not be the "true" zonal wavenumber. Eastward (westward)-propagating diurnal tides are Doppler-shifted up (down) by one zonal wavenumber in the satellite data record. Thus, a wavenumber 4 structure in theory represents DE3 and/or a westward-propagating wavenumber 5 (DW5). The eastward phase "tilt" with height overwhelmingly supports a DE3 interpretation. The reason is that in order for tropospheric tides to transmit energy flux upward, vertical phase progression must be downward in time [*Holton*, 1992, chapter 4]. At a fixed local time, eastward (westward) phase lines slope eastward (westward) with altitude.

[12] The interpretation of the equatorial wavenumber 4 patterns as eastward-propagating diurnal tides is supported by space-time Fourier analysis of lower thermospheric winds. The green line has a nighttime emission in a narrow layer centered at 95 km. Therefore, WINDII samples nearly 24 hours over the 90–110 km range. Figure 3 shows winds collected at 102 km, and between 10°S–10°N binned in longitude and *universal* time. The zonal wind pattern indicates a clear 3-peaked eastward progression over the course of 24 hours. The meridional winds show an eastward tilt that is not as distinct, and no dominant wavenumber

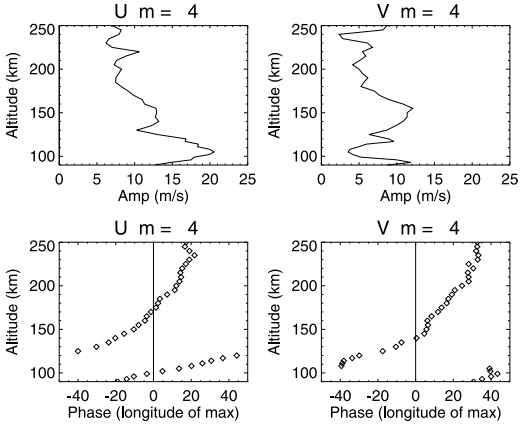

Figure 2. (top) Amplitude and (bottom) phase of $m = 4$ component of (left) zonal and (right) meridional winds.

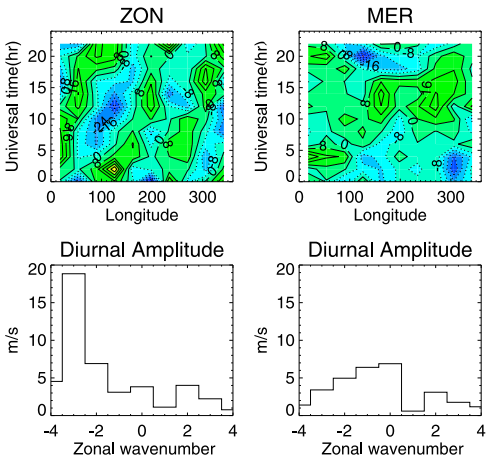

Figure 3. (top left) zonal and (top right) meridional winds at 102 km plotted as a function of longitude and universal time. (bottom) Amplitudes of the longitudinal diurnal harmonics. The migrating component has been filtered from the observations. Negative wavenumbers denote eastward propagation.

structure. Space-time Fourier analysis of the top wind panels was carried out, and the amplitudes of the longitudinal diurnal harmonics are plotted as histograms in Figure 3, bottom. These structures confirm the dominance of DE3 in the zonal wind. The diurnal meridional winds are not dominated by any particular wavenumber; rather, they exhibit a zonally averaged component and a diffuse eastward-propagating spectrum.

[13] In theory, an eastward-propagating semidiurnal tide with zonal wavenumber 2 (SE2) and a stationary zonal wavenumber 4 (SPW 4) would also produce wavenumber-4 patterns in the daytime-(or nighttime-) only wind [*Salby*, 1982]. We therefore examined the zonal wavenumber spectra of the semidiurnal and stationary harmonics in the lower thermosphere where complete local time coverage is available (not shown). We found no significant contribution by either SE2 or SPW 4, so we have confidence in our interpretations of wavenumber 4 zonal winds at 102 km as DE3 tides. However, this does not preclude the possibility that SE2 could attain more importance at higher altitudes [*Häusler and Lühr*, 2009].

[14] Figures 1–3 have focused on the structure of wavenumber 4 at the equator. We now examine its global structure, reconstructed at 90°E. Figure 4 shows that the zonal wind has a very broad meridional extent that is centered on the equator. A vertical half-wavelength of about 20 km is suggested in the MLT region, based on the distance between minimum and maximum zonal wind values at low latitudes. These characteristics are consistent with the classical predictions for diurnal Kelvin waves [*Longuett-Higgins*, 1967].

[15] Meridional winds exhibit antisymmetrical structures, with symmetric structure developing above 140 km. Meridional wind values are significantly weaker than the zonal winds below 150 km, where the zonal winds show broad symmetry below. This behavior further confirms the interpretation of zonal wavenumber 4 as largely a DE3 Kelvin wave below 150 km. The symmetric meridional winds at higher altitudes and the presence of asymmetries in the zonal wind suggests the possibility that higher-order DE3 Hough modes could be present [*Talaat and Lieberman*, 1999]. However, the latitudinal fine structures must be interpreted with caution, as these could be artifacts of multi-year data binning.

3. Summary and Concluding Remarks

[16] We have presented observations of zonal wavenumber 4 in the 90–270 km range inferred from UARS/WINDII. The wave is strongest in the lower thermospheric

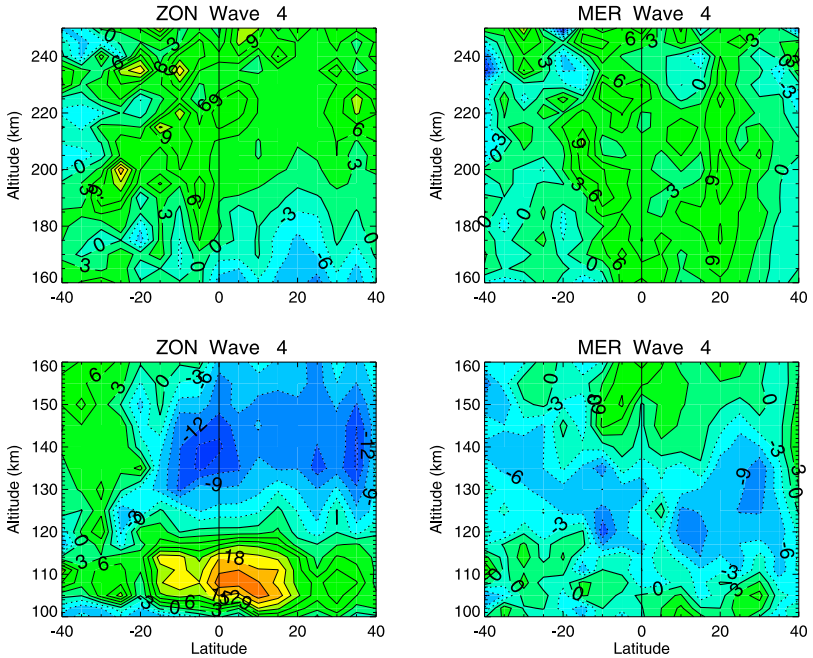

Figure 4. Latitude versus altitude plot of the $m = 4$ (left) zonal and (right) meridional wind, reconstructed at 90°E. Note the different vertical scales between the top and the bottom plots.

equatorial zonal wind, but is also coherent in the meridional wind. Zonal wind amplitudes of 10 m s^{-1} persist up to 250 km. The wave is strongest in the equinox seasons, and in September–October–November. We interpret this signature as DE3 viewed from the satellite perspective.

[17] The evidence of direct propagation of DE3 into the thermosphere has significant implications for the interpretation of in-situ neutral density and wind measurements in the thermosphere. Previously, latitudinal structure of neutral mass density has been shown to be organized along geomagnetic coordinates [*Liu et al.*, 2005], suggesting possible ion-neutral interaction. *Lühr et al.* [2007] also showed significant longitudinal variability in the in-situ neutral zonal wind. They concluded from comparing the phase at the dip equator with that at the equatorial ionization anomaly (EIA) peaks that it was unlikely that ion-neutral coupling was the cause of the longitudinal variations. This paper finds clear evidence of the propagation of nonmigrating tides up to the middle of the F-region. As such, it can effect the longitudinal variability observed in the in-situ neutral measurements independently of the EIA.

[18] **Acknowledgments.** The authors gratefully acknowledge the services of the Goddard Earth Sciences Data and Information Services Center in archiving and distributing UARS data. We thank our reviewers for their helpful suggestions. This research was supported by NASA contracts NNX06AC40G and NNH06CC31C.

References

Burrage, M. D., N. Arvin, W. R. Skinner, and P. B. Hays (1994), Observations of the O_2 atmospheric band nightglow by the High Resolution Doppler Imager, *J. Geophys. Res.*, *99*, 15,017–15,023.

Chapman, S., and R. S. Lindzen (1970), *Atmospheric Tides*, Gordon and Breach, New York.

Emmert, J. T., B. J. Fejer, C. G. Fesen, G. G. Shepherd, and B. H. Solheim (2001), Climatology of middle- and low-latitude daytime F region disturbance neutral winds measured by Wind Imaging Interferometer (WINDII), *J. Geophys. Res.*, *106*, 24,701–24,712.

England, S. L., T. J. Immel, E. Sagawa, S. B. Henderson, M. E. Hagan, S. B. Mende, H. U. Frey, C. M. Swenson, and L. J. Paxton (2006), Effect of atmospheric tides on the morphology of the quiet time, post-sunset equatorial ionospheric anomaly, *J. Geophys. Res.*, *111*, A10S19, doi:10.1029/2006JA011795.

Forbes, J. M., M. E. Hagan, X. Zhang, and K. Hamilton (1997), Upper atmosphere tidal oscillations due to latent heat release in the tropical troposphere, *Ann. Geophys.*, *15*, 1165–1175.

Forbes, J. M., S. L. Bruinsma, X. Zhang, and J. Oberheide (2009), Surface-exosphere coupling due to thermal tides, *Geophys. Res. Lett.*, *36*, L15812, doi:10.1029/2009GL038748.

Gault, W. A., et al. (1996), Validation of O(^1S) wind measurements by WINDII: The WIND Imaging Interferometer on UARS, *J. Geophys. Res.*, *101*, 10,405–10,430.

Hagan, M. E., and J. M. Forbes (2002), Migrating and nonmigrating diurnal tides in the middle and upper atmosphere excited by tropospheric latent heat release, *J. Geophys. Res.*, *107*(D24), 4754, doi:10.1029/2001JD001236.

Hagan, M. E., A. Maute, R. G. Roble, A. D. Richmond, T. J. Immel, and S. L. England (2007), Connections between deep tropical clouds and the Earth's ionosphere, *Geophys. Res. Lett.*, *34*, L20109, doi:10.1029/2007GL030142.

Häusler, K., and H. Lühr (2009), Nonmigrating tidal signals in the upper thermospheric zonal wind at equatorial latitudes as observed by CHAMP, *Ann. Geophys.*, *27*, 2643–2652.

Hays, P. B., D. Wu, M. D. Burrage, D. A. Gell, H. Grassl, R. S. Lieberman, A. R. Marshall, Y. T. Morton, D. Ortland, and W. R. Skinner (1994), Observations of the diurnal tide from space, *J. Atmos. Sci.*, *51*, 3077–3093.

Holton, J. R. (1992), *An Introduction to Dynamic Meteorology*, 3rd ed., Academic, San Diego, Calif.

Immel, T. J., E. Sagawa, S. L. England, S. B. Henderson, M. E. Hagan, S. B. Mende, H. U. Frey, C. M. Swenson, and L. J. Paxton (2006), Control of equatorial ionospheric morphology by atmospheric tides, *Geophys. Res. Lett.*, *33*, L15108, doi:10.1029/2006GL026161.

Kil, H., E. R. Talaat, S.-J. Oh, L. J. Paxton, S. L. England, and S.-Y. Su (2008), Wave structures of the plasma density and vertical **E** × **B** drift in low-latitude *F* region, *J. Geophys. Res.*, *113*, A09312, doi:10.1029/2008JA013106.

Lieberman, R. S., and P. B. Hays (1994), An estimate of the momentum deposition in the lower thermosphere by the observed diurnal tide, *J. Atmos. Sci.*, *51*, 3094–3105.

Lieberman, R. S., D. A. Ortland, and E. S. Yarosh (2003), Climatology and interannual variability of diurnal water vapor heating, *J. Geophys. Res.*, *108*(D3), 4123, doi:10.1029/2002JD002308.

Lieberman, R. S., D. M. Riggin, D. A. Ortland, S. W. Nesbitt, and R. A. Vincent (2007), Variability of mesospheric diurnal tides and tropospheric diurnal heating during 1997–1998, *J. Geophys. Res.*, *112*, D20110, doi:10.1029/2007JD008578.

Liu, H., H. Lühr, V. Henize, and W. Köhler (2005), Global distribution of the thermospheric total mass density derived from CHAMP, *J. Geophys. Res.*, *110*, A04301, doi:10.1029/2004JA010741.

Longuett-Higgins, M. S. (1967), The eigenfunctions of Laplace's tidal equations over a sphere, *Philos. Trans. R. Soc. London, Ser. A*, *269*, 511–607.

Lühr, H., K. Häusler, and C. Stolle (2007), Longitudinal variation of F region electron density and thermospheric zonal wind caused by atmospheric tides, *Geophys. Res. Lett.*, *34*, L16102, doi:10.1029/2007GL030639.

Lühr, H., M. Rother, K. Häusler, P. Alken, and S. Maus (2008), The influence of nonmigrating tides on the longitudinal variation of the equatorial electrojet, *J. Geophys. Res.*, *113*, A08313, doi:10.1029/2008JA013064.

McLandress, C., and W. E. Ward (1994), Tidal/gravity wave interactions and their influence on the large-scale dynamics of the middle atmosphere: Model results, *J. Geophys. Res.*, *99*, 8139–8155.

McLandress, C., G. G. Shepherd, B. H. Solheim, M. D. Burrage, P. B. Hays, and W. R. Skinner (1996a), Combined mesosphere/lower thermosphere winds using WINDII and HRDI data from the Upper Atmosphere Research Satellite, *J. Geophys. Res.*, *101*, 10,441–10,453.

McLandress, C., G. G. Shepherd, and B. H. Solheim (1996b), Satellite observations of thermospheric tides: Results from the wind imaging interferometer on UARS, *J. Geophys. Res.*, *101*, 4093–4114.

Oberheide, J., and J. M. Forbes (2008a), Thermospheric nitric oxide variability induced by nonmigrating tides, *Geophys. Res. Lett.*, *35*, L16814, doi:10.1029/2008GL034825.

Oberheide, J., and J. M. Forbes (2008b), Tidal propagation of deep tropical cloud signatures into the thermosphere from TIMED observations, *Geophys. Res. Lett.*, *35*, L04816, doi:10.1029/2007GL032397.

Oberheide, J., Q. Wu, T. L. Killeen, M. E. Hagan, and R. G. Roble (2006), Diurnal nonmigrating tides from TIMED Doppler Interferometer wind data: Monthly climatologies and seasonal variations, *J. Geophys. Res.*, *111*, A10S03, doi:10.1029/2005JA011491.

Oberheide, J., J. M. Forbes, K. Häusler, Q. Wu, and S. L. Bruinsma (2009), Tropospheric tides from 80 to 400 km: Propagation, interannual variability, and solar cycle effects, *J. Geophys. Res.*, *114*, D00I05, doi:10.1029/2009JD012388.

Sagawa, E., T. J. Immel, H. U. Frey, and S. B. Mende (2005), Longitudinal structure of the equatorial anomaly in the nighttime ionosphere observed by IMAGE/FUV, *J. Geophys. Res.*, *110*, A11302, doi:10.1029/2004JA010848.

Salby, M. L. (1982), Sampling theory for asynoptic satellite observations. Part I: Space-time spectra, resolution, and aliasing, *J. Atmos. Sci.*, *39*, 2577–2601.

Svoboda, A. A., J. M. Forbes, and S. Miyahara (2005), A space-based climatology of MLT diurnal winds, temperatures and densities from UARS wind measurements, *J. Atmos. Sol. Terr. Phys.*, *67*, 1533–1543.

Talaat, E. R., and R. S. Lieberman (1999), Nonmigrating diurnal tides in mesospheric and lower thermospheric winds and temperatures, *J. Atmos. Sci.*, *56*, 4073–4087.

Zhang, X., J. M. Forbes, M. E. Hagan, J. M. Russell III, S. E. Palo, C. J. Mertens, and M. G. Mlynczak (2006), Monthly tidal temperatures 20–120 km from TIMED/SABER, *J. Geophys. Res.*, *111*, A10S08, doi:10.1029/2005JA011504.

R. S. Lieberman, Colorado Research Associates Division, Northwest Research Associates, 3380 Mitchell Ln., Boulder, CO 80301, USA.

E. R. Talaat, Johns Hopkins University Applied Physics Laboratory, 11100 Johns Hopkins Rd., Laurel, MD 20723, USA. (elsayed.talaat@jhuapl.edu)